

Article

Inclusions and Gemological Characteristics of Emeralds from Kamakanga, Zambia

Yi Zhang and Xiao-Yan Yu *

School of Gemology, China University of Geosciences Beijing, Beijing 100083, China

* Correspondence: yuxy@cugb.edu.cn

Abstract: Currently, Zambia is one of the world's major emerald-producing countries. In this study, emerald samples from Kamakanga, Zambia, were systematically analyzed by standard gemological tests, microscopic observation, Raman spectroscopy test of mineral inclusions, and fluid inclusions. The study found Kamakanga emeralds have higher RI (refractive index) and SG (specific gravity) than average. The common inclusions in Kamakanga emeralds are pseudo-hexagonal, dark green, brownish, or oval platelet phlogopite; red spot or skeletal hematite; black spot, platelet, or dendritic oxide inclusions (pyrolusite, magnetite, ilmenite); or schorl. The common paragenetic mineral is schorl. Other mineral inclusions are fluorapatite, tremolite, and calcite. All Kamakanga emeralds contain at least two kinds of common mineral inclusions that are described above, and the characteristic mineral inclusions are pseudo-hexagonal dark green platelet phlogopite and a large quantity of fluorapatite. The fluorapatite inclusions with colorless transparent rims and greyish hazy interiors are reported for the first time. Most fluid inclusions in Kamakanga emeralds are rectangular two- or three-phase inclusions, containing gas phase ($\text{CO}_2 + \text{CH}_4 + \text{H}_2\text{O}$ or CO_2), aqueous fluid, and sometimes solid phase (carbonate). A small number of hexagonal three-phase fluid inclusions can be seen in Kamakanga emeralds, containing gas phase ($\text{CO}_2 + \text{CH}_4$), aqueous fluid, and daughter crystals (siderite).

Keywords: Zambian emeralds; inclusions; gemological characteristics; Raman spectroscopy



Citation: Zhang, Y.; Yu, X.-Y. Inclusions and Gemological Characteristics of Emeralds from Kamakanga, Zambia. *Minerals* **2023**, *13*, 341. <https://doi.org/10.3390/min13030341>

Academic Editor: Pierre Schiano

Received: 25 January 2023

Revised: 17 February 2023

Accepted: 23 February 2023

Published: 28 February 2023



Copyright: © 2023 by the authors. Licensee MDPI, Basel, Switzerland. This article is an open access article distributed under the terms and conditions of the Creative Commons Attribution (CC BY) license (<https://creativecommons.org/licenses/by/4.0/>).

1. Introduction

Emerald is a variety of beryl whose ideal formula is $\text{Be}_3\text{Al}_2[\text{Si}_2\text{O}_6]_3$. Emeralds are loved for their vibrant and beautiful color and have a long history of use as a gem [1]. Colombian emeralds have been synonymous with high quality emeralds for centuries, but with the emergence of high quality emeralds from other deposits around the world, Zambian emeralds have also become popular as the second most important origin by value after Colombia [2,3]. Zambian emeralds tend to have a darker green color than Colombian [4], but it is difficult to distinguish Zambian emerald from others with the naked eye, just by color.

In the past two decades, Zambia has accounted for approximately 40% of the world's production of emeralds [5,6]. In October 2017, Gemfield announced that the auction of Zambian emeralds had earned \$21.5 million, including a 6100 carat rough emerald. Consequently, Zambian emeralds have great promising in terms of both quality and production. Zambian emeralds are mainly produced from two areas: Musakashi and Kafubu. Kamakanga is one of the emerald deposits in Kafubu area.

Although emerald deposits were discovered in the Kafubu area of Zambia as early as 1928, the geological setting was only researched and reported after 1982 [5–8], then mentioned it was several times in comparisons [9–12]. Subsequently, studies began to explore the geochronology of the Kafubu emerald area [13–15]. The Kafubu area of Zambia has approximately 19 emerald deposits, and the mechanized mining activities are mostly concentrated on the Kagem, Grizzly, Chantete, and Kamakanga deposits. As the research

has progressed over the years, experts and scholars have studied the gemological, spectroscopic, and chemical elements of Zambian Kafubu emeralds, but the samples from the Kamakanga deposit were too few compared with other mechanized mining deposits of Kagem, Grizzly, and Chantete [2,4,16].

In this study, we updated information on the geological settings of Kamakanga, Zambia, and selected the samples from this deposit. We used standard gemological tests, microscopic observation, and Raman spectra of inclusions to illustrate the characteristics of Kamakanga emeralds with a view to summarizing and supplementing previous research on them and providing a new basis for the identification of Kamakanga emeralds.

2. Geological Settings

The Kafubu area is located in north-central Zambia and the southern part of the Coppebelt, which is the center of the transcontinental Pan-African belt in central–south Africa, separating the Congo Kraton to the north and the Kalahari to the south (Figure 1). The rocks of the Kafubu area have evolved in three successive orogenic events (ca. 500–2000 Ma [million years ago]): the Ubendian, Irumide, and Lufilian [17].

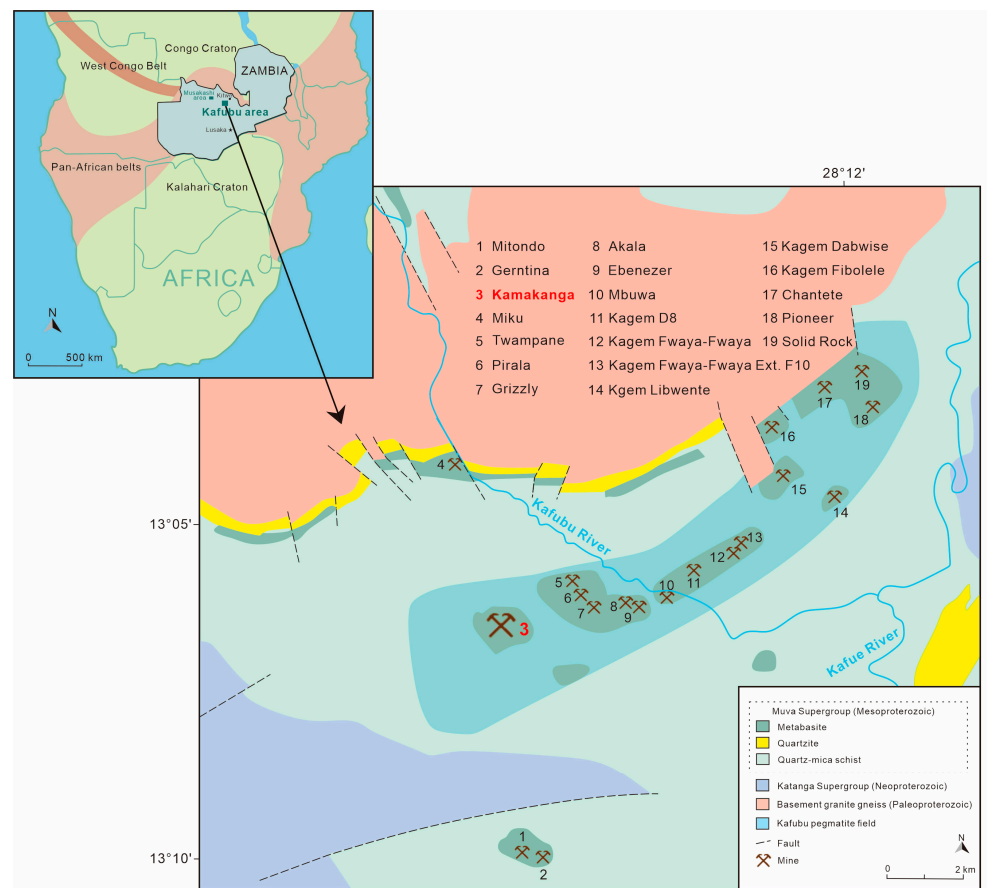


Figure 1. Simplified geological map of the Kafubu area, including the location of the Kamakanga deposit in this area. Modified from [2].

The Kafubu area has approximately 19 deposits, and the Kamakanga deposit is on the south side of the Kafubu River (Figure 1). According to the new classification scheme introduced by Giuliani et al. [9], the Kamakanga emerald deposit belongs to the type IA (tectonic-magmatic-related in mafic-ultramafic rocks). The Kamakanga deposit is hosted by the Cr rich metabasite (3000–4000 ppm) of the Muva Supergroup. The Muva Supergroup consists of Metabasite, Quartzite, and Quartz mica schist. The metabasite contains talc chlorite±actinolite±magnetite schists. This metabasite is a metamorphosed volcanic rock, mainly consisting of komatiites (i.e. highly magnesian ultramafic rocks), which is rich

in chromium content and provides the necessary component for emerald mineralization. In addition, the metabasite is overlapped by a major field of Be bearing pegmatite and hydrothermal veins nearly 20 km long.

During the late Pan-African orogeny (c. 530 Ma), beryllium -bearing pegmatites and hydrothermal veins intruded various crustal units. The emerald mineralisation is formed by the metasomatic alteration of the metabasites containing Cr by fluids containing Be [2,6]. In short, the emeralds in the Kamakanga deposit are formed through the interaction of pegmatites with ultramafic country rocks [10]. The emeralds with economic value are almost completely limited to the phlogopite reaction zones (approximately 0.5–3 m wide) between quartz-tourmaline veins and the metabasites [2].

3. Materials and Methods

A total of 27 rough crystal emeralds from Kamakanga, Zambia, ranging from 0.20 to 4.90 ct, were analyzed for the study (Figure 2). The samples were obtained from the owner of the local mine. The majority of the studied samples appeared as well-formed hexagonal columns, or slabs developed along {0001}, while a few were fragments. The transparency of the studied samples was highly variable, being slightly transparent to transparent. The main color of the samples was green and partially showed a slightly bluish-green color.

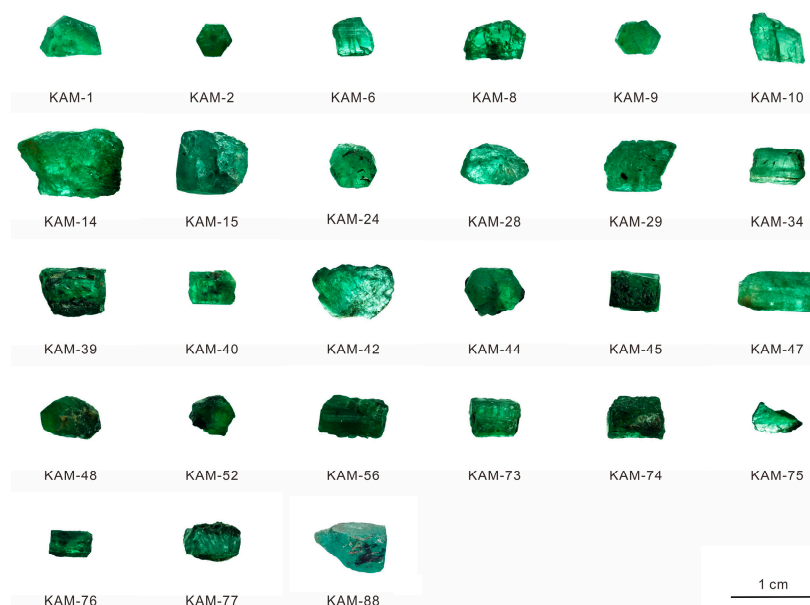


Figure 2. The 27 Kamakanga, Zambia, emerald samples for this study.

The standard gemological tests for the samples were conducted at the Gemological Research Laboratory of the China University of Geosciences (Beijing). All the samples were investigated with a refractometer, a Chelsea filter, a long-wave (365 nm) and short-wave (254 nm) UV lamp, DiamondView™, and an apparatus for hydrostatic-specific gravity testing. Internal and external features were observed with a GI-MP22 gemological photographic microscope using darkfield, brightfield, and top illumination.

Inclusions were identified using a WITec Alpha 300R confocal Raman microscope in the Innovation Academy for Earth Science, Chinese Academy of Science, with the laser operating at 488 nm excitation (blue), between 4000 and 100 cm^{-1} , the integration time of 3 s, accumulating up to two scans, and actual laser power of 6–10 mW. The laser spot size was 1 μm . The Raman shifts were calibrated using monocrystalline silicon before the test, with a tolerance of $\pm 0.5 \text{ cm}^{-1}$.

4. Results

4.1. Conventional Gemological Properties

Vertical lines, round growth hillocks (Figure 3a), and etchpits (Figure 3b) were common on the surface of Kamakanga emerald columns. Red Fe oxide impurities dipped on the surface of the crystal (Figure 3c) and in the internal inclusions. Color zones were common in Kamakanga emeralds with hexagonal color zones perpendicular to the **C axis**, which varies in width and color ranging from light to dark green, with two or more layers (Figure 3d).

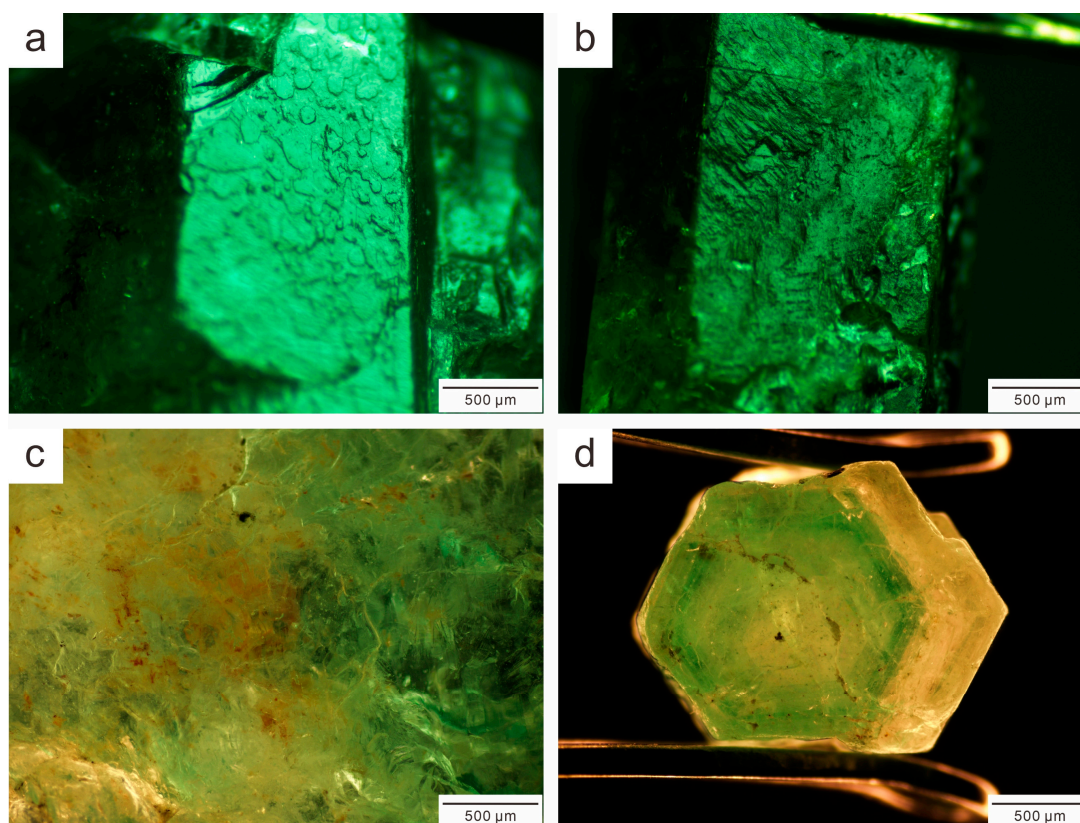


Figure 3. (a) Round growth hillocks on the surface of emerald column (KAM-1); (b) Etchpits on the surface of emerald column (KAM-45); (c) Red Fe oxide impurities on the surface of emerald (KAM-14); (d) Hexagonal color zones in emerald (KAM-9).

The emeralds from Kamakanga had a refractive index of 1.585–1.602 (n_e : 1.585–1.593 and n_o : 1.592–1.602) with birefringence between 0.007 and 0.009, and specific gravity of 2.74–2.81. Turning emerald samples 360° under a polariscope, the emeralds appear four times bright and four times dark. Dichroism was medium light green or green (o-ray) and bluish green (e-ray). The visible spectra of most emeralds from the spectroscope had distinct lines in the red region (approximately 680 nm), partial absorption in the orange and yellow region (between 580 and 620 nm), and complete absorption in the violet region (<460 nm). Through the Chelsea filter, all the emeralds appeared dark green. The emeralds were typically inert to long- and short-wave UV radiation. The gemological properties of emeralds from Kamakanga are summarized in Table 1.

Table 1. Gemological properties of emeralds from Kamakanga, Zambia.

Properties	Results
Color	Light to dark green and bluish green
Clarity	Medium to heavy included
Refractive indices	n_e : 1.585–1.593; n_o : 1.592–1.602
Birefringence	0.007–0.009
Specific gravity	2.74–2.81
Pleochroism	Medium-light green or green (o-ray) and bluish-green (e-ray)
Fluorescence	Typically inert
Chelsea filter	Dark green
Visible spectrum	Distinct lines at the red region (approximately 680 nm), partial absorption in the orange and yellow region (between 580 and 620 nm), and complete absorption in the violet region (<460 nm)
Internal features	<ul style="list-style-type: none"> Partially healed fissures with various shapes of two and three phase fluid inclusions, but typically rectangular or hexagonal Mineral inclusions (this study): oval shape brownish or pseudo-hexagonal green platelet of phlogopite, red spot or skeletal hematite, black spot or platelet or dendritic oxide, tremolite, fluorapatite, calcite, schorl Inclusions described by other authors: talc, barite, albite, actinolite, chlorite, quartz, fluorite, carbonate (magnesite, siderite, ankerite, calcite), rutile, zircon, beryl, pyrite [2,4,16,18,19] Hexagonal color zones perpendicular to the C axis vary in width and color, ranging from light to dark green, with two or more layers

4.2. Inclusions under the Gem Microscope

4.2.1. Mineral Inclusions

Mineral inclusions were common in the Kamakanga emeralds. The following three kinds of mineral inclusions were common mineral inclusions, and all Kamakanga emerald samples contained at least two kinds of common and different mineral inclusions: the first was phlogopites, occurring with a brownish color and oval shapes (Figure 4a) and pseudo-hexagonal dark green platelets (Figure 4b), which were identified by Raman analysis; the second was red spot or skeletal hematites (Figure 4c), which were identified by Raman analysis; the third was black spots (Figure 4a), or platelets and dendritic oxide inclusions (Figure 4d). According to previous studies, it was presumed to be pyrolusite, magnetite, or ilmenite [2,4]. However, the dendritic oxide inclusions were seen in other schist-hosted emeralds too [4]. Schorl was the most common paragenetic mineral.

Less abundant than those common mineral inclusions were black prism tremolites with diamond-shaped cross-sections (Figure 5a), and fluorapatite inclusions were rare in the emerald samples. All the above inclusions were identified by Raman analysis. Interestingly, although fluorapatite inclusions were rare in most of the emerald samples, they occurred numerically in only one sample (KAMA-8): crystal inclusions with colorless transparent rims and a greyish hazy interior (Figure 5b); clusters consisting of a large number of small colorless transparent hexagonal prisms and hexagonal bipyramids (Figure 5c); green hexagonal prisms or plate crystal inclusions; colorless transparent plate crystals infiltrated with red Fe oxide impurities (Figure 5d); transparent crystal inclusions with different sizes and round shapes; colorless and transparent crystal particles.

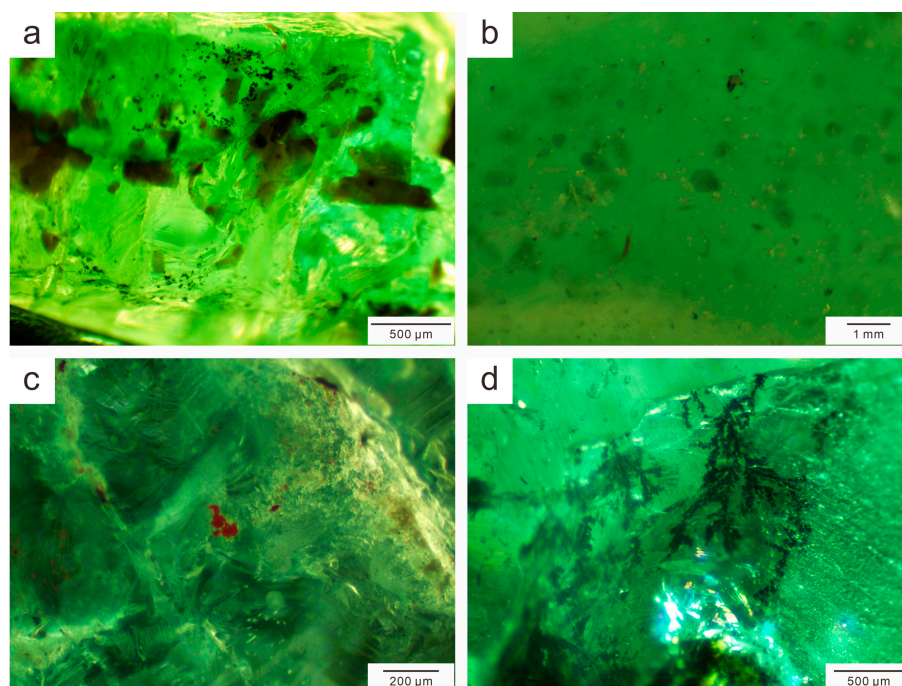


Figure 4. (a) Brownish platelet phlogopites and black spot oxide inclusions in emerald (KAM-6); (b) Pseudo-hexagonal green platelet phlogopites in emerald (KAM-88); (c) An irregularly shaped platelet hematite in emerald (KAM-42); (d) Black dendritic oxide inclusions in emerald (KAM-15).

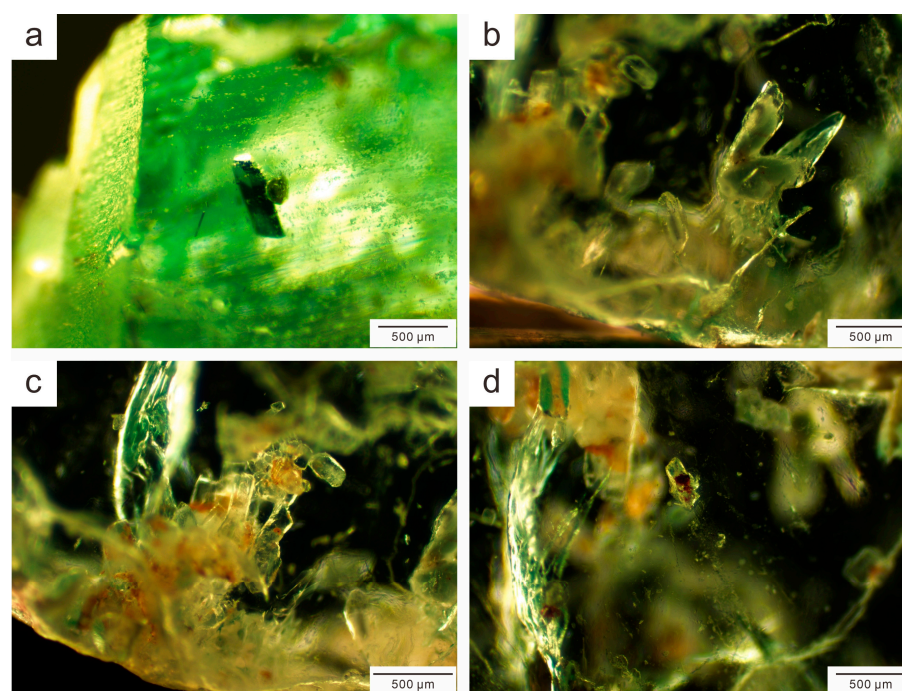


Figure 5. (a) Black prism tremolite in emerald (KAM-15); (b) Fluorapatite inclusions with colorless, transparent rim and a greyish, hazy interior in emerald (KAM-8); (c) Colorless transparent fluorapatite cluster in emerald (KAM-8); (d) Colorless plate crystals infiltrated with red Fe oxide impurities in emerald (KAM-8).

4.2.2. Fluid Inclusions

There were abundant blocky fluid inclusions (approximately 50–150 μm) with rectangular shapes and fractures in Kamakanga emeralds. A large number of rectangular fluid

inclusions were arranged parallel to each other. Some of them were parallel to the **C axis** (Figure 6a), while others were oblique to it. These rectangular fluid inclusions generally contained either two phases (liquid and gas) or three phases (liquid, gas, solid). The most common blocky fluid inclusions were two- or three-phase rectangular fluid inclusions (Figure 6b), next to three-phase hexagonal fluid inclusions (approximately 60–160 μm) (Figure 6c). Partially hexagonal fluid inclusions were parallel or partially perpendicular to the **C axis** and had distinct hexagonal boundaries. These hexagonal fluid inclusions contained three phases (liquid, gas, and solid).

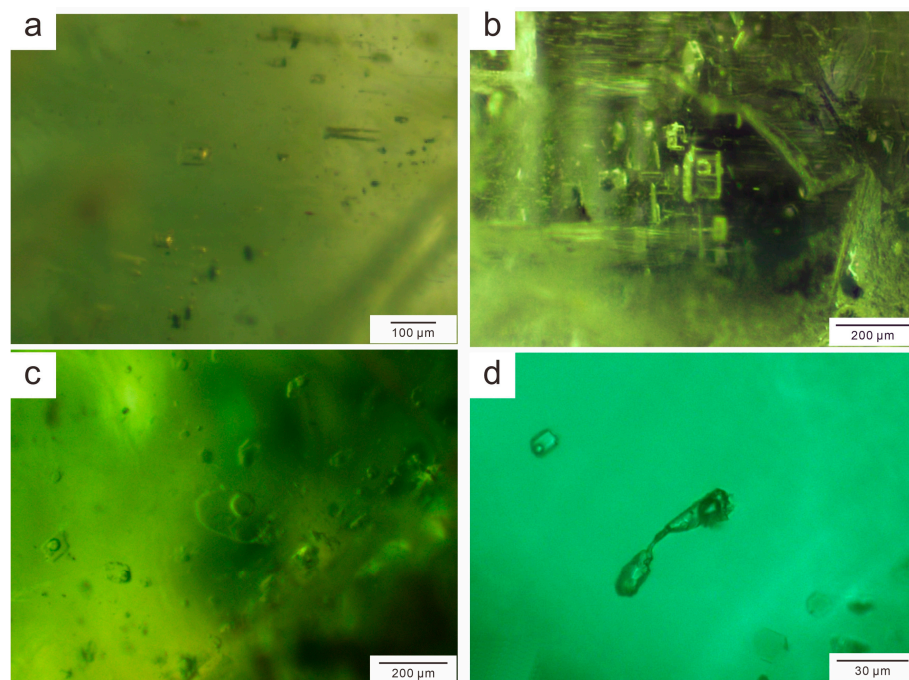


Figure 6. (a) Paralleling rectangular fluid inclusions in emerald (KAM-24); (b) Rectangular fluid inclusions in emerald (KAM-34); (c) Hexagonal fluid inclusions in emerald (KAM-44); (d) Necked-down, irregularly shaped fluid inclusion in emerald (KAM-44).

At room temperature, the majority of the bubbles in the fluid inclusions were large, round, or squeezed into ovals, and gas bubbles appeared to occupy one-third to one-half the volume of the fluid inclusions. Few bubbles in the fluid inclusions were relatively small and round. In addition, rare fluid inclusions in the Kamakanga emeralds showed necked-down, irregular shapes (Figure 6d).

4.3. Raman Spectra Characteristics

4.3.1. The Raman Spectra of the Kamakanga Emeralds

In order to remove the interference of the emerald absorption peaks in the analysis of the Raman spectra of the inclusions, we tested the main crystal of samples by Raman spectroscopy before the tests for internal inclusions.

By comparing the Raman spectra of the emeralds (KAM-8, KAM-29, KAM-44, KAM-77) with those in the literature [20–22], we found the following characteristic peaks in the range of 100–4000 cm^{-1} : a weak absorption peak at 330 cm^{-1} caused by the Al–O outer bending vibration; an absorption peak at 404 cm^{-1} caused by the Al–O outer deformation vibration; a weak absorption peak at 522 cm^{-1} caused by the O–Be–O outer bending vibration; a strong absorption peak at 689 cm^{-1} caused by the Si–O–Si internal deformation vibration; an absorption peak at 1010 cm^{-1} caused by the Be–O outer non-bridging oxygen expansion vibration; an absorption peak at 1072 cm^{-1} caused by the Si–O and/or Be–O stretching vibration; a strong absorption peak at 3600 cm^{-1} caused by the type II H_2O expansion vibration. The attribution of the Raman signal at 689 cm^{-1} and 1010 cm^{-1} is

still controversial. Some experts believe that 698 cm^{-1} is caused by the Be–O stretching vibrations [23–25], and 1010 cm^{-1} is caused by the Si–O stretching vibration [24,25].

The observations of the current study are in good agreement with these previous findings. The peak positions of the emerald samples studied in this paper are shown in Table 2.

Table 2. Peak positions of the emeralds (cm^{-1}).

Sample Number	Emerald Characteristic Peak Range						Channel Water Absorption Peak Range		Data Source
							Type II H ₂ O	Type I H ₂ O	
KAM-8	328	403	-	686	998	1068	3600	-	this paper
KAM-44	-	405	529	691	1004	1071	3602	-	this paper
KAM-77	330	409	522	691	1010	1071	3602	-	this paper
RRUFF (R050065)	323	400	-	685	1002	1067	-	-	RRUFF
Emeralds	323	398	-	685	1011	1068	3600	3610	[22]

4.3.2. The Raman Spectra of Mineral Inclusions

Mineral inclusions were common in Kamakanga emeralds, such as phlogopite, hematite, fluorapatite, tremolite, calcite, and schorl. All of the mineral inclusions were identified by Raman by comparison with the RRUFF standard database.

Phlogopite and hematite were common inclusions in the emeralds. Brownish platelets of phlogopites appeared within the emeralds or exposed to the surface of the emeralds (KAM-6). Green pseudo-hexagonal platelets of phlogopite were found near or on the surface of the emeralds (KAM-88). Red spot hematites were usually clustered together, while skeletal platelet hematites occurred singly (KAM-8).

Raman analyses revealed that the platelet inclusion on the surface of sample KAM-6 (Figure 7a) was made up of phlogopite (peaks at 189, 275, 325, 678, 1084 cm^{-1}) (Figure 7b). Sample KAM-88 had a large number of dark green pseudo-hexagonal inclusions (Figure 7c), and the sizes were approximately 600 μm . The Raman spectrum of one of them (Figure 7d) showed the fundamental vibrations of phlogopite (peaks at 191, 278, 682 cm^{-1}). The results are consistent with the species of micas in the altered metabasite host rock as documented by Seifert et al. [6].

Also common were skeletal platelets (Figure 7e) that provided Raman spectra (Figure 7f) consistent with hematite (peaks at 225, 293, 408, 494, 613 cm^{-1}) in sample KAM-8.

Fluorapatite inclusions were rare in most of the emerald samples, but numerous apatite inclusions were observed in ZAM-8. All of the following fluorapatite inclusions were from KAM-8.

Figure 8a shows two positions in an inclusion: the colorless transparent rim of the inclusion (P1) and the greyish hazy interior of the inclusion (P2). The results of the separate Raman analysis are shown in Figure 8b: Raman spectra in P1 and P2 both had the characteristic Raman shifts for fluorapatite (peaks at 431, 590, 966, 1052 cm^{-1} and 428, 589, 962, 1051 cm^{-1}). This kind of fluorapatite inclusion is reported for the first time. In addition, the cluster consisted of a large number of colorless hexagonal prisms and hexagonal bipyramids (approximately 250 μm). One of the hexagonal bipyramids (Figure 8c) was tested by Raman spectroscopy with the characteristic Raman shifts of fluorapatite (Figure 8d): 431, 590, 961, 1052, 1079 cm^{-1} . The colorless crystal inclusions were divided into large and small sizes (Figure 8e): the larger ones (approximately 100 μm) were generally approximately round in shape, while the smaller ones (approximately 25 μm) were square. Raman spectra (Figure 8f) of these crystal inclusions showed that both the larger and small inclusions were fluorapatite (peaks at 431, 590, 966, 1052, 1079 cm^{-1}). Figure 8g shows two positions in a colorless transparent plate inclusion containing red impurities: a colorless transparent plate of the inclusion (F1) and red impurities (F2). The Raman spectrum (Figure 8h) in F1 had fundamental vibrations at 428, 591, 964, and nd

1051 cm^{-1} , which were characteristic Raman shifts for fluorapatite. F2 showed fundamental vibrations at 211 cm^{-1} , and 271 cm^{-1} , identified by the Raman database as Fe oxide.

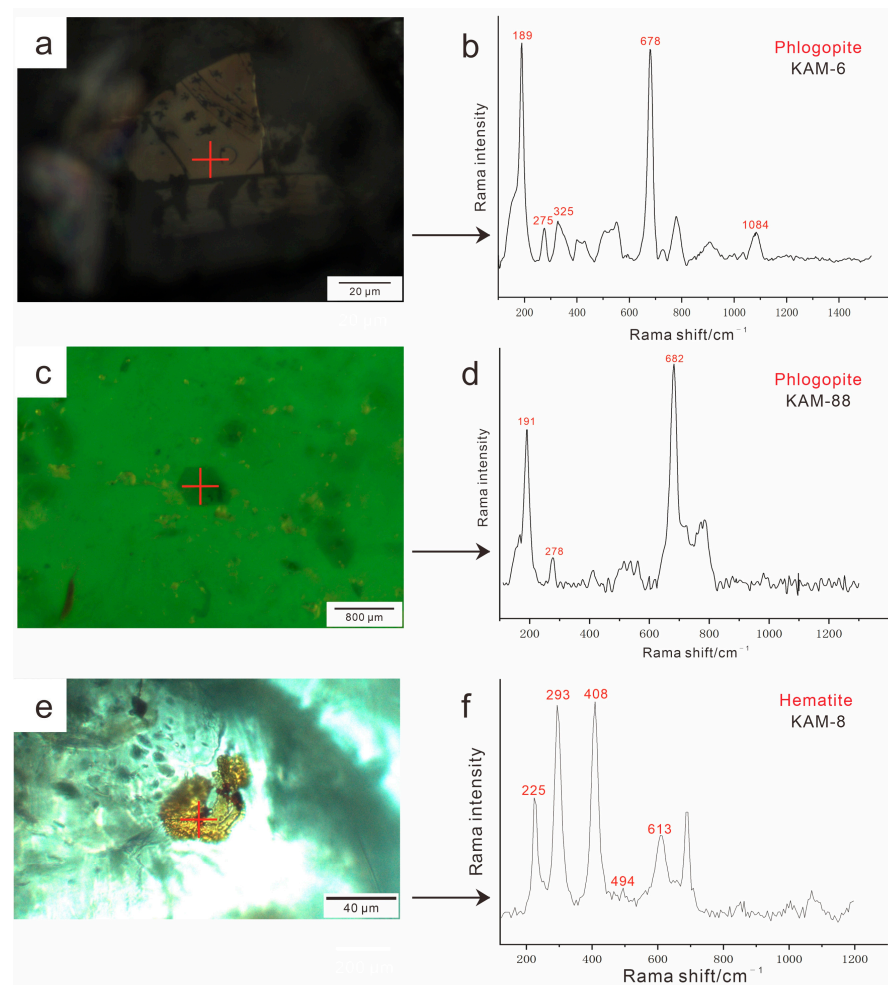


Figure 7. (a) Phlogopite inclusion in a Kamakanga emerald (KAM-6) and (b) its Raman spectrum. (c) Phlogopite inclusion in Kamakanga emerald (KAM-88) and (d) its Raman spectrum. (e) Hematite inclusion in Kamakanga emerald (KAM-8) and (f) its Raman spectrum.

There were long blue-green prisms with diamond-shaped cross sections inclusions in Kamakanga emerald KAM-88 (Figure 9a). These inclusions, which passed from the surface to the interior of the sample, were identified by Raman spectra as tremolite, with characteristic Raman shifts of 120, 156, 178, 222, 231, 390, 521, 671, 929, 1025, and 1056 cm^{-1} (Figure 9b).

A tiny particle inclusion (Figure 9c) of approximately 6 μm was found in sample KAM-88, which was tested by Raman spectroscopy and showed the characteristic Raman shifts for calcite (peaks at 151, 278, 711, 1084 cm^{-1}) (Figure 9d).

The black mineral with well-formed hexagonal columns (Figure 9e) in Kamakanga emerald (KAM-29) was schorl (peaks at 147, 249, 365, 493, 697, 1043 cm^{-1}) (Figure 9f). Actually, schorl was the most common paragenetic mineral in emeralds samples.

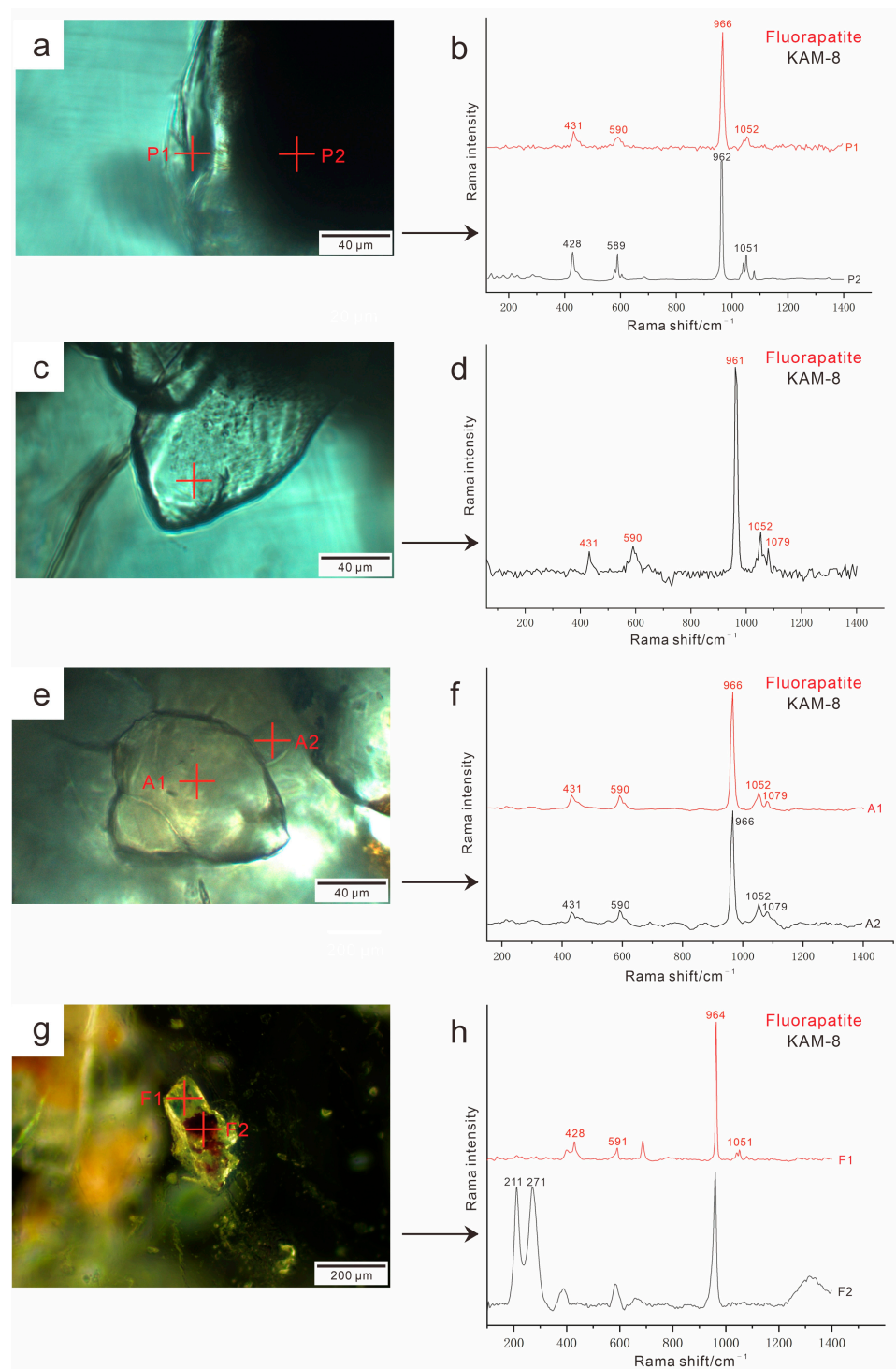


Figure 8. (a–h) Four typical fluorapatite inclusions in Kamakanga emerald (KAM-8) were tested by Raman spectroscopy. The results are shown on the right.

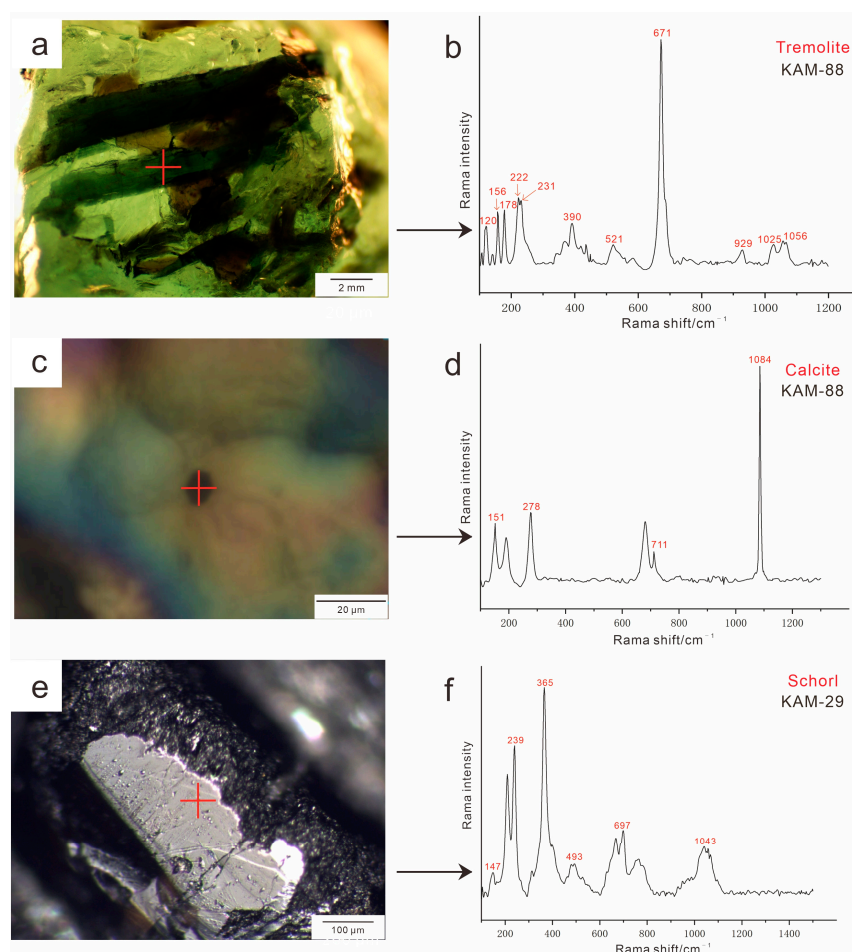


Figure 9. (a) Tremolite inclusion in a Kamakanga emerald (KAM-88) and (b) its Raman spectrum. (c) Calcite inclusion in a Kamakanga emerald (KAM-88) and (d) its Raman spectrum. (e) Schorl inclusion in a Kamakanga emerald (KAM-29) and (f) its Raman spectrum.

4.3.3. The Raman Spectra of Fluid Inclusions

Most of the fluid inclusions in emerald samples were two- or three-phase and rectangular in shape (Figure 6), which is a characteristic of Zambian emeralds [2]. These rectangular fluid inclusions typically hosted a gas bubble and liquid, but some of them also contain a solid phase. However, less abundant than rectangular fluid inclusions were hexagonal three-phase inclusions with distinct boundaries.

There were a large number of rectangular two- or three-phase inclusions in Kamakanga emeralds, and the components of these inclusions were identified by Raman spectra. The gas phases were identified as $\text{CO}_2 + \text{CH}_4 + \text{H}_2\text{O}$ (Figure 10) or CO_2 (Figure 11) (CO_2 : 1286 and 1390 cm^{-1} ; CH_4 : 2919 cm^{-1} ; H_2O : 1620 cm^{-1}). The solid phase was tentatively identified by optical means as carbonate. The liquid phases were identified as water (a band at 3400 cm^{-1}).

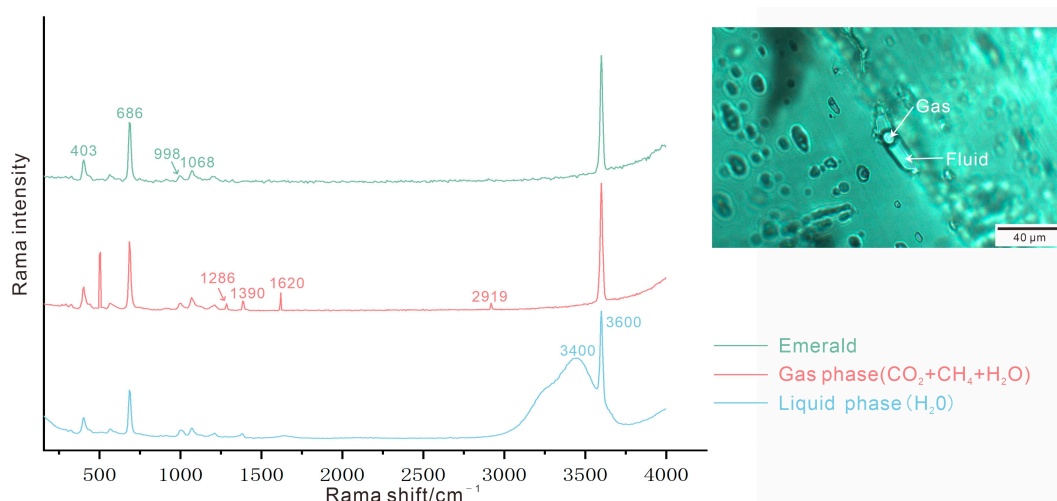


Figure 10. This rectangular two-phase inclusion in Kamakanga emerald (KAM-8) clearly displays a gas bubble. Raman spectroscopy was used to identify the host emerald (green), the $\text{CO}_2 + \text{CH}_4 + \text{H}_2\text{O}$ gas bubble (red), and the liquid phase (blue). The spectra are stacked for clarity.

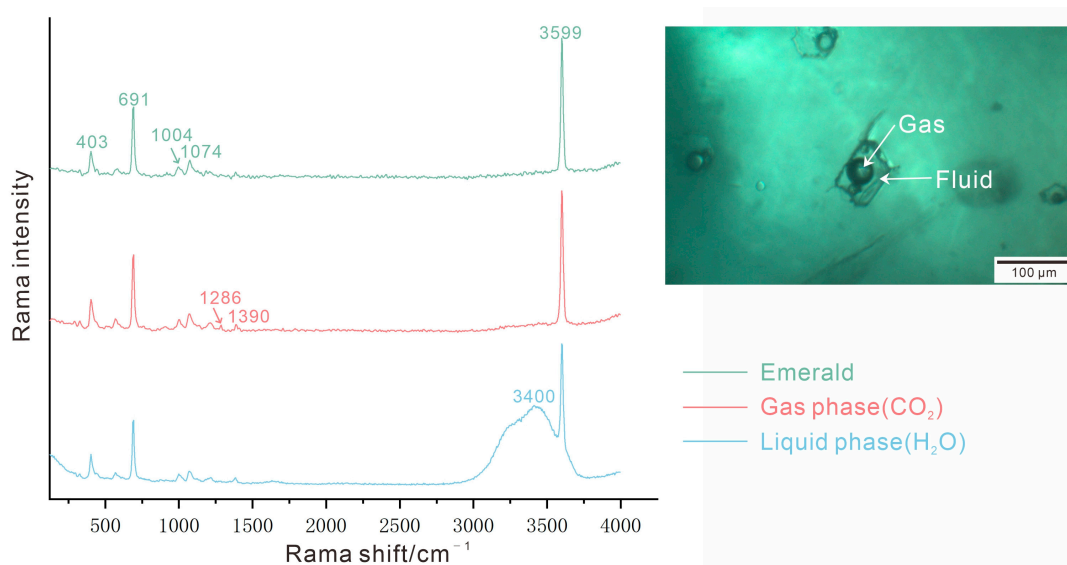


Figure 11. This rectangular three-phase inclusion in a Kamakanga emerald (KAM-44) clearly displays a gas bubble and a colorless crystal. Raman spectroscopy was used to identify the host emerald (green), the CO_2 gas bubble (red), and the liquid phase (blue). The spectra are stacked for clarity.

Hexagonal three-phase inclusions were less abundant than rectangular fluid inclusions. The composition of gas bubbles was not detected but was presumed to be $\text{CO}_2 + \text{CH}_4$ based on other hexagonal fluid inclusion test results in this paper. Daughter crystals were identified as siderite (peaks at 287, 713, and 1090 cm^{-1}) (Figure 12). The liquid phases were identified as water (a band at 3400 cm^{-1}).

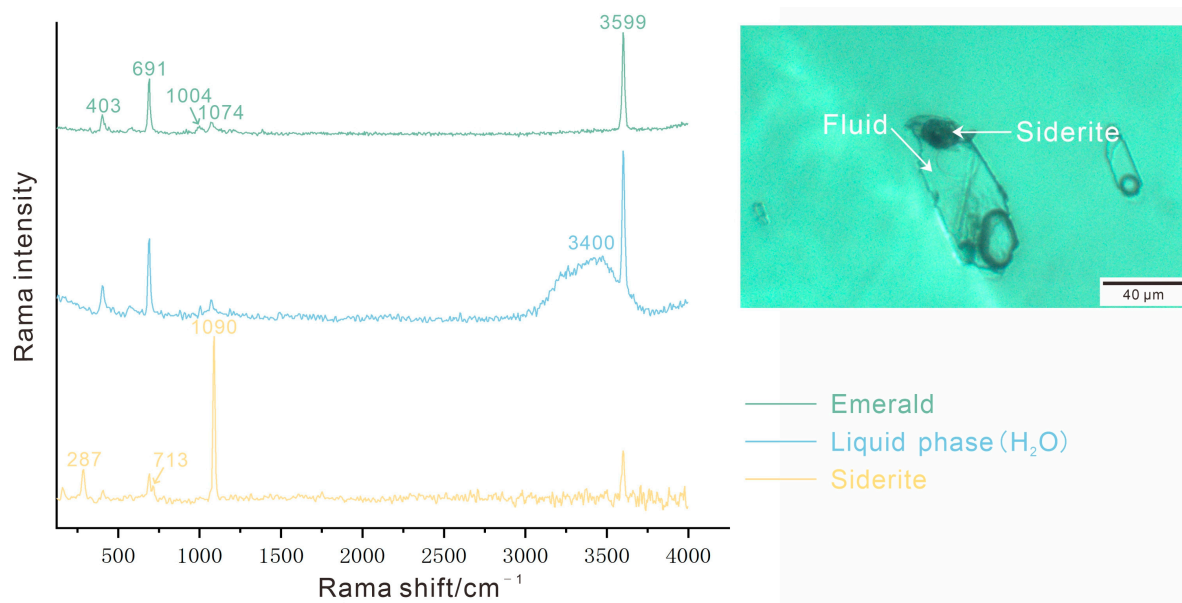


Figure 12. This hexagonal three-phase inclusion in a Kamakanga emerald (KAM-44) clearly displays a gas bubble and a black mineral. Raman spectroscopy was used to identify the host emerald (green), the liquid phase (blue), and the siderite crystal (yellow). The spectra are stacked for clarity.

5. Discussion

5.1. Gemological Characteristics

Most Kamakanga emeralds have well-formed hexagonal columns. Most emerald samples have an evenly distributed green color or bluish-green color, while some samples display color banding ranging from light to deep green perpendicular to the **C** axis.

The RI, SG, dichroism, fluorescence, and special optical properties (such as appearing dark green under the Chelsea filter) of the samples are consistent with the properties of the Kafubu emeralds studied by Zwaan [2]. However, according to the new classification scheme introduced by Giuliani et al. [9], emerald deposits are divided into two main types and seven sub-types depending on their geological environment. Compared with emeralds from Kamakanga and other types of deposits (Table 3), Kamakanga emeralds have higher RI and SG for two reasons. First, Kamakanga emeralds have higher alkali metal content [2]. The Raman spectroscopy test conclusion that Kamakanga emeralds have type II H₂O can support the first reason. Second, Kamakanga emeralds have high Fe content. The optical property causing all the emeralds to appear dark green under the Chelsea filter can support the second reason. To a limited extent, these features can help distinguish between Zambian emeralds and emeralds from other origins (Table 3).

Table 3. Gemological properties of emeralds from various sources.

Type of Deposit	Country	Deposits	Refractive Indices			SG	Chelsea Filter	Date Source	
			N _e	N _o	Birefringence				
Tectonic-magmatic-related	Type IA	Zambia	Kamakanga	1.585–1.593	1.592–1.602	0.007–0.009	2.74–2.81	Inert	this paper
		Zambia	Kafubu	1.578–1.591	1.585–1.599	0.006–0.009	2.71–2.78	Inert	[2]
		Russia	Ural	1.575–1.584	1.581–1.591	0.007	2.72–2.75	Weak pink	[26]
		Zimbabwe	Sandawana	1.584–1.587	1.590–1.594	0.006–0.007	2.74–2.77	Pink	[27]
		India	Rajasthan	1.578–1.585	1.585–1.590	0.005–0.012	2.68–2.72	Inert	[28]
		Brazil	Fazenda Bonfim	1.578–1.583	1.587–1.591	0.008–0.009	2.72–2.74	Inert or pink to red	[29]
		China	Dayakou	1.575–1.582	1.581–1.589	0.005–0.008	2.64–2.72	Inert	[30]
Type IC	Nigeria	Kaduna	1.560–1.569	1.566–1.574	0.005–0.006	2.64–2.68	Inert	[31]	

Table 3. Cont.

Type of Deposit	Country	Deposits	Refractive Indices			SG	Chelsea Filter	Date Source	
			N_e	N_o	Birefringence				
Tectonic-metamorphic-related	Type IIA	Brazil	Santa Terezinha de Goiás	1.580–1.587	1.590–1.593	0.005–0.012	2.71–2.79	Inert	[32]
	Type IIB	Colombia	All	1.570–1.573	1.576–1.580	0.006–0.008	2.69–2.71	Pink to strong pink	[16,33]
	Type IIC	China	Davdar	1.576–1.580	1.583–1.585	0.005–0.008	2.64–2.76	Inert	[34,35]
		Afghanistan	Panjshir	1.572–1.580	1.580–1.590	0.007–0.010	2.65–2.71	Inert or pink	[16,36]
Type IID	Pakistan	Swat	1.580–1.589	1.587–1.600	0.006–0.011	2.70–2.82	Pink to red	[37]	

5.2. Inclusion Characteristics

Kamakanga emeralds have abundant inclusions and fractures. The common inclusions observed in Kamakanga emeralds are pseudo-hexagonal dark green or oval brownish platelet phlogopite; red spot or skeletal hematite; black spot, platelet, or dendritic oxide inclusion (pyrolusite, magnetite, ilmenite) [2,4]; and the common paragenetic mineral is schorl. All Kamakanga emerald samples contain at least two kinds of common and different mineral inclusions. Compared with the above common mineral inclusions, tremolite is relatively uncommon in emeralds. Fluorapatite and calcite are rare in Kamakanga emeralds. Previous studies confirm that phlogopite, red skeletal hematite, and fluorapatite are characteristic inclusions of Zambia Kafubu emeralds [2]. Kamakanga is one of the emerald deposits in the Kafubu area. Combining the geological background of the Kamakanga deposit, this paper finds that green pseudo-hexagonal dark green platelet phlogopite and the large quantity of fluorapatite inclusions are characteristic of Kamakanga emeralds, and schorl and pseudo-hexagonal dark green platelet phlogopites are associated minerals of emerald.

Inclusions can reflect geological settings [38,39]. A large number of schorls and phlogopites in emeralds confirms that the mineralization of emeralds at Kamakanga is directly related to phlogopite exocontact of quartz-tourmaline veins. Actually, the best emeralds are found in phlogopite schist near intersections of the pegmatite veins and quartz-tourmaline [2]. In addition, the pseudo-hexagonal dark green platelet phlogopite inclusions are syngenetic inclusions and the oval brownish platelet phlogopite inclusions are protogenetic, indicating that phlogopites formed before or at the same time as the emeralds. However, brownish platelet phlogopite inclusions were also observed in Indian, Brazilian, Russian, and Ethiopian emeralds. In contrast, pseudo-hexagonal dark green platelet phlogopite inclusions have not been reported in other origins, so pseudo-hexagonal dark green platelet phlogopites are characteristic inclusions of Kamakanga emeralds.

The emeralds in the Kamakanga deposit are formed through the interaction of pegmatites with ultramafic country rocks, and hematite is the accessory mineral of pegmatites [6,10]. Large quantities of hematite can reflect these geological settings. Red spots or skeletal hematite are characteristic inclusions of Kafubu emeralds, but not of Kamakanga emeralds. Because these inclusions are not only found in emeralds from the Kamakanga deposit, they also occur in emeralds from many other emerald deposits in the Kafubu area [2]. Consequently, red spot or skeletal hematite inclusions are common but not characteristic inclusions in Kamakanga emeralds.

In addition, the abundance of tremolite, fluorapatite, and calcite in emeralds can reflect their content in the surrounding rocks. Compared with common mineral inclusions, tremolite is relatively uncommon in emerald samples, while fluorapatite and calcite are rare in emerald samples. Actually, tremolite is one of the major minerals, while fluorapatite and calcite are the minor minerals from the rocks hosting emerald mineralizations [6]. Interestingly, a large number of fluorapatite inclusions were observed in only one sample (KAM-8) in this paper, while rare in others, indicating that fluorapatite crystals are locally distributed in the surrounding rocks. Actually, fluorapatite locally with white crystals and crystal aggregates up to 5 mm long in phlogopite and quartz-beryl-phlogopite-tourmaline

veins [6]. Furthermore, the quantity of fluorapatite in KAM-8 is 90% of the total number of inclusions in this sample. Consequently, the large quantity of fluorapatite inclusions is a characteristic of Kamakanga emeralds. The fluorapatite inclusions with colorless transparent rims and greyish hazy interiors are reported for the first time. Raman results for both the rim and interior parts of the inclusions were apatite. Consequently, we speculate that the rims are well-crystallized fluorapatite and the interiors are bad-crystallized fluorapatite.

Emeralds are often divided into two broad groups according to fluid inclusions (blocky and jagged), which roughly correspond to the two main types (tectonic-magmatic-related and tectonic-metamorphic related) in the new emerald classification scheme [4,9]. Blocky fluid inclusions also suggest the Kamakanga deposit belongs to the tectonic-magmatic related type. Most of the blocky fluid inclusions in Kamakanga emeralds are two- or three-phase rectangular. A small number of hexagonal three-phase fluid inclusions can be seen in Kamakanga emeralds. The fluid inclusion characteristics and components of the Kamakanga emeralds studied in this paper are shown in Table 4.

Table 4. Fluid inclusion characteristics and components in Kamakanga emeralds.

Shape	Size	Phase	Component
rectangular	50–150 μm	two-phase	gas phase: $\text{CO}_2 + \text{CH}_4 + \text{H}_2\text{O}$ liquid phase: H_2O
		three-phase	gas phase: CO_2 liquid phase: H_2O solid phase: Carbonate
hexagonal	60–160 μm	three-phase	gas phase: $\text{CO}_2 + \text{CH}_4$ liquid phase: H_2O solid phase: Siderite

According to the similar geological genesis, emeralds from Zambia (Kamakanga), India, Brazil, Russia, and Ethiopia have similar blocky fluid inclusions (rectangular two-phase inclusions) and solid inclusions (Brown phlogopite protogenetic inclusions). However, the rectangular fluid inclusions of Indian emeralds have only two phases, whereas Zambian emeralds have three phases. In addition, Indian emeralds have CO_2 in the liquid phase of some hexagonal fluid inclusions, whereas Zambian emeralds do not [28]. Brazilian emeralds have parallel tiny tubes described as “rain-like,” which are not found in Zambian emeralds [4]. The blocky fluid inclusions in Ethiopian emeralds contain two separate liquid phases whereas Zambian emeralds contain only one [40]. Iridescent thin films that lie parallel to the basal pinacoid are a unique feature of Russian emeralds [41]. In short, it is possible to distinguish Zambian (Kamakanga) from Indian, Ethiopian, Brazilian, and Russian emeralds by these characteristics.

6. Conclusions

Overall, Kamakanga emeralds showed some special optical properties, mineral inclusions, and fluid inclusion characteristics.

Kamakanga emeralds have higher RI and SG, which may be explained by higher alkali metal content and high Fe content. Both test results that emeralds only showed type II H_2O in Raman spectra and that they appeared dark green under the Chelsea filter support this conclusion. Color zones were common in Kamakanga emeralds.

The common mineral inclusions in Kamakanga emeralds are pseudo-hexagonal dark green or oval brownish platelet phlogopite; red spot or skeletal hematite; black spot, platelet, or dendritic oxide inclusions. The common paragenetic mineral is schorl. All Kamakanga emerald samples contain at least two kinds of common and different mineral inclusions. Other inclusions are fluorapatite, tremolite, and calcite. The fluorapatite inclusions with colorless transparent rims and greyish hazy interiors are reported for the first time. Combined with the geological settings, the characteristic mineral inclusions of

Kamakanga emeralds are pseudo-hexagonal dark green platelet phlogopites and a large quantity of fluorapatite.

Most fluid inclusions in Kamakanga emeralds are two or three phase rectangular inclusions (gas phase: CO₂ + CH₄ + H₂O or CO₂; aqueous fluid; solid phase: carbonate). A small number of hexagonal three-phase fluid inclusions (gas phase: CO₂ + CH₄; aqueous fluid; solid phase: siderite) can be seen in Kamakanga emeralds.

Author Contributions: Conceptualization, Y.Z. and X.-Y.Y.; methodology, Y.Z. and X.-Y.Y.; software, Y.Z.; validation, Y.Z. and X.-Y.Y.; formal analysis, Y.Z. and X.-Y.Y.; investigation, Y.Z. and X.-Y.Y.; resources, X.-Y.Y.; data curation, Y.Z.; writing—original draft preparation, Y.Z.; writing—review and editing, Y.Z. and X.-Y.Y.; visualization, Y.Z. and X.-Y.Y.; funding acquisition, X.-Y.Y. All authors have read and agreed to the published version of the manuscript.

Funding: This study was financially supported by a project from the China Geological Survey (DD20190379-88).

Data Availability Statement: All data generated or used during the study appear in the submitted article.

Acknowledgments: We are grateful to Ming-Ke Wu and Xiao-Guang Li for their support and technical guidance in Raman spectroscopy test. The authors are grateful to Li-Jie Qin and Yun You for constructive comments.

Conflicts of Interest: The authors declare no conflict of interest.

References

1. Harrell, J. Archaeological geology of the world's first emerald mine. *Geosci. Can.* **2004**, *31*, 69–76.
2. Zwaan, J.H.; Seifert, A.V.; Vrána, S.; Laurs, B.M.; Ankar, B.; Simmons, W.B.S.; Falster, A.U.; Lustenhouwer, W.J.; Muhlmeister, S.; Koivula, J.I.; et al. Emeralds from the Kafubu Area, Zambia. *Gems Gemol.* **2005**, *41*, 117–148.
3. Giuliani, G.; France-Lanord, C.; Coget, P.; Schwarz, D.; Cheilletz, A.; Branquet, Y.; Giard, D.; Martin-Izard, A.; Alexandrov, P.; Piat, D.H. Oxygen isotope systematics of emerald: Relevance for its origin and geological significance. *Miner. Deposita* **1998**, *33*, 513–519. [[CrossRef](#)]
4. Saeseaw, S.; Renfro, N.D.; Palke, A.C.; Sun, Z.; McClure, S.F. Geographic origin determination of emerald. *Gems Gemol.* **2019**, *55*, 614–646. [[CrossRef](#)]
5. Mashikinyi, M. Investigating the Technical, Financial and Regulatory Challenges in the Zambian Gemstone Mining Sector: A Case Study of Gemcanton Investment Holdings Limited. Ph.D. Thesis, The University of Zambia, Lusaka, Zambia, 2020.
6. Seifert, A.V.; Žáček, V.; Vrána, S.; Pecina, V.; Zachariáš, J.; Zwaan, J.C. Emerald mineralization in the Kafubu area, Zambia. *Bull. Geosci.* **2004**, *79*, 1–40.
7. Koivula, J.I. Tourmaline as an inclusion in Zambian emeralds. *Gems Gemol.* **1982**, *18*, 225–227. [[CrossRef](#)]
8. Sliwa, A.S.; Nguluwe, C.A. Geological setting of Zambian emerald deposits. *Precambrian Res.* **1984**, *25*, 213–228. [[CrossRef](#)]
9. Giuliani, G.; Groat, L.A.; Marshall, D.; Fallick, A.E.; Branquet, Y. Emerald deposits: A review and enhanced classification. *Minerals* **2019**, *9*, 105. [[CrossRef](#)]
10. Giuliani, G.; Groat, L.A. Geology of corundum and emerald gem deposits: A Review. *Gems Gemol.* **2019**, *55*, 464–489. [[CrossRef](#)]
11. Long, Z.Y.; Yu, X.Y.; Jiang, X.; Guo, B.J.; Ma, C.Y.; You, Y.; Zheng, Y.Y. Fluid boiling and fluid-rock interaction as primary triggers for emerald deposition: Insights from the Dayakou emerald deposit (China). *Ore Geol. Rev.* **2021**, *139*, 104454. [[CrossRef](#)]
12. Zheng, Y.Y.; Yu, X.Y.; Guo, H.S. Major and trace element geochemistry of dayakou vanadium-dominant emerald from malipo(Yunnan, China): Genetic model and geographic origin determination. *Minerals* **2019**, *9*, 777. [[CrossRef](#)]
13. Viana, R.R.; Mänttari, I.; Kunst, H.; Jordt-Evangelista, H. Age of pegmatites from eastern Brazil and implications of mica intergrowths on cooling rates and age calculations. *J. S. Am. Earth Sci.* **2003**, *16*, 493–501. [[CrossRef](#)]
14. Behling, S.; Wilson, W.E. The Kagem emerald mine: Kafubu Area, Zambia. *Mineral. Rec.* **2010**, *41*, 59–68.
15. Ren, J.P.; Wang, J.; Zuo, L.B.; Liu, X.Y.; Dai, C.C.; Xu, K.K.; Li, G.Z.; Geng, J.Z.; Xiao, Z.B.; Sun, K.; et al. Zircon U–Pb and biotite 40Ar/39Ar geochronology from the Anzan emerald deposit in Zambia. *Ore Geol. Rev.* **2017**, *91*, 612–619. [[CrossRef](#)]
16. Saeseaw, S.; Pardieu, V.; Sangsawong, S. Three-phase inclusions in emerald and their impact on origin determination. *Gems Gemol.* **2014**, *50*, 114–133. [[CrossRef](#)]
17. John, T.; Schenk, V.; Mezger, K.; Tembo, F. Timing and PT evolution of whiteschist metamorphism in the Lufilian Arc–Zambezi Belt Orogen (Zambia): Implications for the assembly of Gondwana. *J. Geol.* **2004**, *112*, 71–90. [[CrossRef](#)]
18. Milisenda, C.C.; Malango, V.; Taupitz, K.C. Edelsteine aus Sambia—Teil 1: Smaragd. *Z. Dtsch. Gemmol. Ges.* **1999**, *48*, 9–28.
19. Graziani, G.; Gübelin, E.; Lucchesi, S. The genesis of an emerald from the Kitwe District, Zambia. *Neues Jahrb. Mineral. Mon.* **1983**, *4*, 75–186.

20. Inessa, M.; Michael, R.; Micheline, B.; Gerard, P. Raman microspectroscopy and fluorescence of emeralds from various deposits. *J. Raman Spectrosc.* **2000**, *31*, 485–490.
21. Jehlička, J.; Culka, A.; Bersani, D.; Vandenabeele, P. Comparison of seven portable Raman spectrometers: Beryl as a case study. *J. Raman Spectrosc.* **2017**, *48*, 1289–1299. [[CrossRef](#)]
22. Shen, J.Q.; Hu, Z.K.; Cui, S.Y.; Zhang, Y.F.; Li, E.Q.; Liang, W.; Xu, B. A study on beryl in the Cuonadong Be-W-Sn polymetallic deposit, Longzi County, Tibet, China. *Crystals* **2021**, *11*, 777. [[CrossRef](#)]
23. Huang, Z.; Li, G.; Weng, L.; Zhang, M.L. Gemological and Mineralogical Characteristics of Emerald from Ethiopia. *Crystals* **2023**, *13*, 233. [[CrossRef](#)]
24. Bersani, D.; Azzi, G.; Lambruschi, E.; Barone, G.; Mazzoleni, P.; Raneri, S.; Longobaedo, U.; Lottici, P.P. Characterization of emeralds by micro-Raman spectroscopy. *J. Raman Spectrosc.* **2014**, *45*, 1293–1300. [[CrossRef](#)]
25. Adams, D.; Gardner, I.R. Single-crystal vibrational spectra of beryl and diopside. *J. Chem. Soc. Dalton Trans.* **1974**, *14*, 1502–1505. [[CrossRef](#)]
26. Koivula, J.I.; Kammerling, R.C.; DeGhionno, D.; Reinitz, I.; Fritsch, E.; Johnson, M.L. Gemological investigation of a new type of Russian hydrothermal synthetic emerald. *Gems Gemol.* **1996**, *32*, 32–39. [[CrossRef](#)]
27. Zwaan, J.H.; Kanis, J.; Petsch, E.J. Sandawana Mines, Zimbabwe. *Gems Gemol.* **1997**, *33*, 80–100. [[CrossRef](#)]
28. Qin, L.J.; Yu, X.Y.; Guo, H.S. Fluid Inclusion and Chemical Composition Characteristics of Emeralds from Rajasthan Area, India. *Minerals* **2022**, *12*, 641. [[CrossRef](#)]
29. Zwaan, J.C.; Jacob, D.E.; Häger, T.; Neto, M.T.; Kanis, J. Emeralds from the Fazenda Bonfim Region, Rio Grande do Norte, Brazil. *Gems Gemol.* **2012**, *48*, 2–17. [[CrossRef](#)]
30. Zheng, Y.Y. Spectroscopy Characteristic of Channel Water and Origin Tracing of Dayakou Emerald from Yunan Province. Master's Thesis, China University of Geosciences, Beijing, China, 2020. (In Chinese).
31. Schwarz, D.; Kanis, J.; Kinnaird, J. Emerald and green beryl from Central Nigeria. *J. Gemmol.* **1996**, *25*, 117–141. [[CrossRef](#)]
32. Pulz, G.M.; D'el-Rey Silva, L.J.H.; Barros Neto, L.S. The chemical signature of emeralds from the Campos Verdes-Santa Terezinha Mining District, Goiás, Brazil. *J. Gemmol.* **1998**, *26*, 252–261. [[CrossRef](#)]
33. Yu, X.Y. *Colored Gemmology*, 2nd ed.; Geology Press: Beijing, China, 2016; pp. 151–164.
34. Cui, D.; Liao, Z.T.; Qi, L.J.; Zhong, Q.; Zhou, Z.Y. A Study of Emeralds from Davdar, North-Western China. *J. Gemmol.* **2020**, *37*, 374–392. [[CrossRef](#)]
35. Cui, D.; Liao, Z.T.; Qi, L.J.; Zhou, Z.Y. Update on inclusions in emeralds from Davdar, China. *Gems Gemol.* **2020**, *56*, 543–545.
36. Guo, H.S. Comparison of the Characteristics of Emeralds Between Pakistan and Afghanistan. Master's Thesis, China University of Geosciences, Beijing, China, 2021. (In Chinese).
37. Guo, H.; Yu, X.; Zheng, Y.; Sun, Z.; Ng, M.F.-Y. Inclusion and trace element characteristics of emeralds from Swat Valley, Pakistan. *Gems Gemol.* **2020**, *56*, 336–355. [[CrossRef](#)]
38. Long, Z.Y.; Yu, X.Y.; Zheng, Y.Y. Ore formation of the Dayakou emerald deposit (Southwest China) constrained by chemical and boron isotopic composition of tourmaline. *Ore Geol. Rev.* **2021**, *135*, 104208. [[CrossRef](#)]
39. Yu, X.Y.; Long, Z.Y.; Zhang, Y.; Qin, L.J.; Zhang, C.; Xie, Z.R.; Wu, Y.R.; Yan, Y.; Wu, M.K.; Wan, J.X. Overview of Gemstone Resources in China. *Crystals* **2021**, *11*, 1189. [[CrossRef](#)]
40. Verriest, W.; Wongrawang, P. A gemological description of Ethiopian emeralds. *InColor* **2018**, *40*, 72–73.
41. Palke, A.C.; Lawley, F.J.; Verriest, W.; Wongrawang, P.; Katsurada, Y. The Russian emerald saga: The Mariinsky Priisk mine. *InColor* **2019**, *44*, 36–46.

Disclaimer/Publisher's Note: The statements, opinions and data contained in all publications are solely those of the individual author(s) and contributor(s) and not of MDPI and/or the editor(s). MDPI and/or the editor(s) disclaim responsibility for any injury to people or property resulting from any ideas, methods, instructions or products referred to in the content.